The Astrophysical Journal, 742:61 (15pp), 2011 December 1 doi:10.1088/0004-637X/742/2/61

DISSECTING PHOTOMETRIC REDSHIFT FOR ACTIVE GALACTIC NUCLEUS USING *XMM*- AND *CHANDRA*-COSMOS SAMPLES*

M. Salvato[1], O. Ilbert[2], G. Hasinger[1,3], A. Rau[4], F. Civano[5], G. Zamorani[6], M. Brusa[4], M. Elvis[5], C. Vignali[6,7], H. Aussel[8], A. Comastri[6], F. Fiore[9], E. Le Floc'h[8], V. Mainieri[10], S. Bardelli[6], M. Bolzonella[6], A. Bongiorno[4], P. Capak[11], K. Caputi[12], N. Cappelluti[6], C. M. Carollo[13], T. Contini[14,15], B. Garilli[16], A. Iovino[16], S. Fotopoulou[1], A. Fruscione[5], R. Gilli[6], C. Halliday[17], J.-P. Kneib[2], Y. Kakazu[18], J. S. Kartaltepe[19], A. M. Koekemoer[20], K. Kovac[21], Y. Ideue[22], H. Ikeda[22], C. D. Impey[23], O. Le Fevre[2], F. Lamareille[14,15], G. Lanzuisi[24], J.-F. Le Borgne[14,15], V. Le Brun[14,15], S. Lilly[13], C. Maier[13], S. Manohar[18], D. Masters[18,24], H. McCracken[25], H. Messias[26], M. Mignoli[6], B. Mobasher[27], T. Nagao[22,28], R. Pello[14,15], S. Puccetti[29], E. Perez-Montero[14,15,30], A. Renzini[31], M. Sargent[8], D. B. Sanders[3], M. Scodeggio[16], N. Scoville[18], P. Shopbell[18], J. Silvermann[32], Y. Taniguchi[33], L. Tasca[2], L. Tresse[2], J. R. Trump[34], and E. Zucca[6]

[1] Max Planck Institut für Plasma Physik and Excellence Cluster, 85748 Garching, Germany; mara.salvato@ipp.mpg.de
[2] Laboratoire d'Astrophysique de Marseille (UMR 6110) CNRS Université de Provence, F-13388 Marseille Cedex 13, France
[3] Institute for Astronomy, University of Hawaii, Honolulu, HI 96822, USA
[4] Max Planck Institut für extraterrestrische Physik, D-85748 Garching, Germany
[5] Harvard-Smithsonian Center for Astrophysics, Cambridge, MA 02138 USA
[6] INAF–Osservatorio Astronomico di Bologna, I-40127 Bologna, Italy
[7] Dipartimento di Astronomia Universita' di Bologna, I-40127 Bologna, Italy
[8] CEA/DSM-CNRS, Université Paris Diderot, IRFU/SAp, Orme des Merisiers, 91191, Gif-sur-Yvette, France
[9] INAF-Osservatorio Astronomico di Roma, Monteporzio Roma, Italy
[10] European Southern Observatory, 85748 Garching, Germany
[11] Spitzer Science Center, California Institute of Technology, Pasadena, CA 91125, USA
[12] SUPA, Institute for Astronomy, The University of Edinburgh, Royal Observatory, Edinburgh EH9 3HJ, UK
[13] Department of Physics, Eidgenossiche Technische Hochschule (ETH), CH-8093 Zurich, Switzerland
[14] Institut de Recherche en Astrophysique et Planétologie, CNRS, F-31400 Toulouse, France
[15] IRAP, Université de Toulouse, UPS-OMP, Toulouse, France
[16] INAF–IASF Milano, Milan, Italy
[17] Osservatorio Astrofisico di Arcetri, 50125 Firenze, Italy
[18] California Institute of Technology, MC 105-24, Pasadena, CA 91125, USA
[19] National Optical Astronomy Observatory, Tucson, AZ 85719, USA
[20] Space Telescope Science Institute, Baltimore, MD 21218, USA
[21] Max Planck Institute für Astrophysik, Garching, D-85748, Germany
[22] Graduate School of Science and Engineering, Ehime University, Matsuyama 790-8577, Japan
[23] Steward Observatory, University of Arizona, Tucson, AZ 85721, USA
[24] INAF–IASF Bologna, 40129 Bologna, Italy
[25] Institut d'Astrophysique de Paris, UMR 7095, CNRS, Université Pierre et Marie Curie, F-75014 Paris, France
[26] Centro de Astronomia e Astrofísica da Universidade de Lisboa, Observatorio Astronomico de Lisboa, Tapada da Ajuda, 1349-018 Lisboa, Portugal
[27] Department of Physics and Astronomy, University of California, Riverside, CA 92508, USA
[28] The Hakubi Project, Kyoto University, Kyoto 606-8502, Japan
[29] ASI Science Data Center, 00044, Frascati, Italy
[30] Institute de Astrofísica de Andalucía, CSIC, 18080 Granada, Spain
[31] Dipartimento di Astronomia, Universitá di Padova, Padova, Italy
[32] Institute for the Physics and Mathematics of the Universe (IPMU), University of Tokyo, Chiba 277-8568, Japan
[33] Research Center for Space and Cosmic Evolution, Ehime University, Matsuyama 790-8577, Japan
[34] University of California Observatories/Lick Observatory, University of California, Santa Cruz, CA 95064, USA
Received 2011 June 19; accepted 2011 July 15; published 2011 November 4

ABSTRACT

In this paper, we release accurate photometric redshifts for 1692 counterparts to *Chandra* sources in the central square degree of the Cosmic Evolution Survey (COSMOS) field. The availability of a large training set of spectroscopic redshifts that extends to faint magnitudes enabled photometric redshifts comparable to the highest quality results presently available for normal galaxies. We demonstrate that morphologically extended, faint X-ray sources without optical variability are more accurately described by a library of normal galaxies (corrected for emission lines) than by active galactic nucleus (AGN) dominated templates, even if these sources have AGN-like X-ray luminosities. Preselecting the library on the bases of the source properties allowed us to reach an accuracy $\sigma_{\Delta z/(1+z_{\rm spec})} \sim 0.015$ with a fraction of outliers of 5.8% for the entire *Chandra*-COSMOS sample. In addition, we release revised photometric redshifts for the 1735 optical counterparts of the *XMM*-detected sources over the entire 2 deg^2 of COSMOS. For 248 sources, our updated photometric redshift differs from the previous release by $\Delta z > 0.2$. These changes are predominantly due to the inclusion of newly available deep *H*-band photometry ($H_{\rm AB} = 24$ mag). We illustrate once again the importance of a spectroscopic training sample and how an assumption about the nature of a source together, with the number and the depth of the available bands, influences the accuracy of the photometric redshifts determined for AGN. These considerations should be kept in mind when defining the observational strategies of upcoming large surveys targeting AGNs, such as *eROSITA* at

X-ray energies and the Australian Square Kilometre Array Pathfinder Evolutionary Map of the Universe in the radio band.

Key words: galaxies: active – galaxies: distances and redshifts – methods: data analysis – surveys – techniques: photometric – X-rays: galaxies

Online-only material: color figures, machine-readable tables

1. INTRODUCTION

The scientific yield of current and future systematic studies of large samples of extragalactic sources depends primarily on the observable redshift, which is one of very few observables that can be directly measured. A redshift then indicates the source distance via a cosmological model, and can be used to estimate quantities such as age, black hole (BH) mass, and accretion rate. The constraint of source redshifts has been a primary goal of deep pencil-beam (e.g., HUDF; Williams et al. 1996), wide-area (e.g., *AEGIS*; Davis et al. 2007; COSMOS: Scoville et al. 2007; GOODS: Giavalisco et al. 2004; ECDFS: Lehmer et al. 2005; CFHTLS: Cuillandre & Bertin 2006), as well as future wide-field synoptic sky surveys across the whole electromagnetic spectrum (e.g., *eROSITA*: Predehl et al. 2007; Pan-STARSS: Burgett & Kaiser 2009; LSST: Ivezic et al. 2006; EMU: Norris 2010; *WISE*: Duval et al. 2004). Given the still limited number of multi-objects, near-infrared spectrographs available on large telescopes, comprehensive spectroscopic follow-up studies are generally impractical for deep and large sky surveys and the need for reliable photometric redshifts has arisen.

Thanks to the availability of extensive multi-waveband observations, the accuracy of the photometric redshifts of normal galaxies has dramatically improved over the past decade. The main milestones have been the availability of deep near- and mid-infrared data for the surveys under study, the use of intermediate-band filters that help to increase the spectral resolution of the measured spectral energy distribution (SEDs; Wolf et al. 2001, 2003; Salvato et al. 2009; Ilbert et al. 2009; Cardamone et al. 2010), and the inclusion of emission lines in the template SEDs of normal galaxies (Ilbert et al. 2009; FORS Deep Field: Bender et al. 2001). As a result, we can now estimate the photometric redshifts of normal galaxies with a 2% accuracy (see, e.g., Ilbert et al. 2009; Cardamone et al. 2010).

However, determining accurate and reliable photometric redshifts for sources dominated by an active galactic nucleus (AGN) remains challenging for a number of reasons. First of all, powerful AGNs are dominated by a power-law SED, whose shape produces a color–redshift degeneracy that only a complete and deep multi-wavelength coverage can break (Wolf et al. 2004). Second, the galaxies that host an AGN contribute in most cases to the global SED of the source. The number of possible different types of galaxies and relative host/AGN contributions (as a function of wavelength) is so large that degeneracies between templates and redshifts are unavoidable. Finally, flux variability is an intrinsic property of AGNs that many multi-wavelength surveys do not take into account when planning their observations, leading to problems in achieving a robust SED fit. Only when we correctly account for all these properties will photometric redshifts (hereafter photo-z) for AGNs become more reliable (Salvato et al. 2009; Luo et al. 2010; Cardamone et al. 2010).

Expanding our previous studies (Salvato et al. 2009, hereafter S09) of the photo-z of the *XMM* observations of the entire 2 deg^2 of the COSMOS field (Hasinger et al. 2007; Cappelluti et al. 2009; Brusa et al. 2010), we provide photo-z for the counterparts to ≈1700 *Chandra*-detected sources in the central 0.9 deg^2 (Elvis et al. 2009; Puccetti et al. 2009; F. Civano et al. 2011, in preparation). These *Chandra* data are significantly deeper (by a factor of ∼3–4) than the *XMM* data, and their optical counterparts reach fainter magnitudes (Figure 1). As a consequence, the method developed to compute photo-z for the *XMM*-COSMOS sources needs to be revised before its application to the *Chandra* data set.

Our paper is structured as follows. In Section 2, we present the optical counterparts of our *Chandra* sources, in addition to our photometric and spectroscopic analyses. In Section 3, we repeat the procedure introduced in S09 and split the sample in two subsamples, on the basis of the morphological and variability analysis. In Section 4, we illustrate how we compute the photo-z, extending the technique to faint X-ray sources. We first compute the photo-z using exactly the same procedure as used by S09, showing its limitations (Section 4.1). We then discuss how the results can be improved in the following subsections. In Section 5, we present our results, highlighting the properties of an individual source with $z_{\rm phot} \sim 6.8$ in Section 5.1. General discussion and conclusions, using both *Chandra* and *XMM* sources, are presented in Sections 6 and 7, respectively. Throughout this paper, we use AB magnitudes and assume that $H_0 = 70$ km s^{-1} Mpc^{-1}, $\Omega_\Lambda = 0.7$, and $\Omega_M = 0.3$.

2. THE *CHANDRA*-COSMOS SAMPLE

2.1. Optical and Near-IR Counterparts

The *Chandra*-COSMOS survey (hereafter C-COSMOS; Elvis et al. 2009) is a large (1.8 Ms) *Chandra* program covering the central 0.5 deg^2 of the COSMOS field (centered at 10 hr, +02°) with an effective exposure of ∼160 ks, and an outer 0.4 deg^2 area with an effective exposure of ∼80 ks. The limiting depths of the point-source detections are 1.9×10^{-16} erg cm^{-2} s^{-1} in the soft (0.5–2 keV) band, 7.3×10^{-16} erg cm^{-2} s^{-2} in the hard (2–10 keV) band, and 5.7×10^{-16} erg cm^{-2} s^{-1} in the full (0.5–10 keV) band.

* Based on observations by the Chandra X-ray Observatory Center, which is operated by the Smithsonian Astrophysical Observatory for and on behalf of the National Aeronautics Space Administration under contract NAS8-03060. Also based on observations with the NASA/ESA *Hubble Space Telescope*, obtained at the Space Telescope Science Institute, which is operated by AURA Inc., under NASA contract NAS 5-26555. Also based on observations made with the *Spitzer Space Telescope*, which is operated by the Jet Propulsion Laboratory, California Institute of Technology, under NASA contract 1407. Also based on data collected at the Subaru Telescope, which is operated by the National Astronomical Observatory of Japan; the *XMM-Newton*, an ESA science mission with instruments and contributions directly funded by ESA Member States and NASA; the European Southern Observatory under Large Program 175.A-0839, Chile; the Kitt Peak National Observatory, Cerro Tololo Inter-American Observatory and the National Optical Astronomy Observatory, which are operated by the Association of Universities for Research in Astronomy, Inc. (AURA), under cooperative agreement with the National Science Foundation; the Canada–France–Hawaii Telescope with MegaPrime/MegaCam operated as a joint project by the CFHT Corporation, CEA/DAPNIA, the NRC and CADC of Canada, the CNRS of France, TERAPIX, and the University of Hawaii.

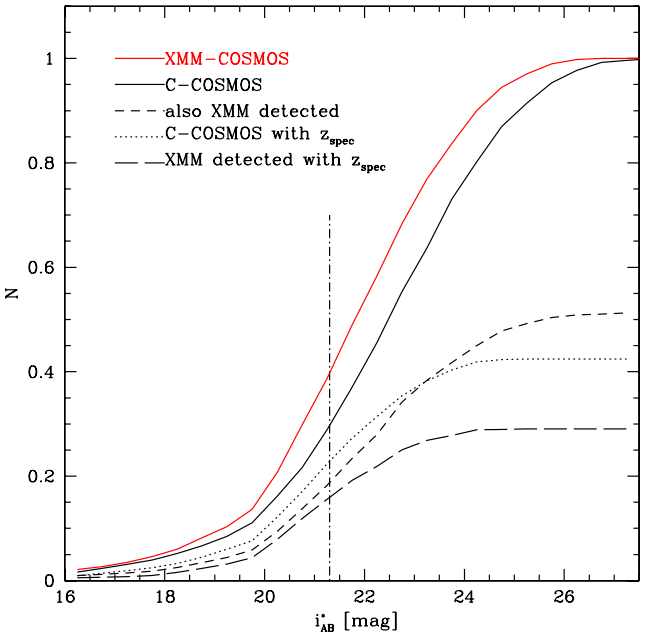

Figure 1. Normalized cumulative i^*_{AB} magnitude distribution for the optical counterparts of the *Chandra*- (black solid line) and *XMM*- (red solid line) COSMOS sources. The distribution of sources common to both samples is also indicated (black dashed line). The dotted curve indicates the C-COSMOS subsample with reliable spectroscopic redshifts, while the long-dashed curve indicates the C-COSMOS sources with spectroscopic redshifts and in common with the *XMM*-COSMOS sample. The vertical line represents the average magnitude of the spectroscopic sample available for C-COSMOS.

A total of 1761 X-ray point sources were detected in our *Chandra* data (for details on the source detection procedure, see Puccetti et al. 2009). The X-ray catalog was presented in Elvis et al. (2009). The optical/NIR counterparts were identified on the basis of a maximum likelihood (ML) ratio technique applied to our optical (Capak et al. 2007), near-infrared (McCracken et al. 2010), and *Spitzer*/Infrared Array Camera (IRAC; Sanders et al. 2007; Ilbert et al. 2010) catalogs, and are presented in F. Civano et al. (2011, in preparation), together with an overall analysis of the sample properties. In summary, thanks to this multi-wavelength identification approach, 1753 counterparts to our X-ray sources (i.e., 99.6%) have been successfully identified in optical/IR bands. Of these 1753, 42 are nearby stars or sources that are too close to a star to be detected separately; these stellar sources are not considered in this paper.

For completeness, we provide in Figure 1 the normalized cumulative i^*_{AB} magnitude distribution for the optical counterparts to C-COSMOS (black solid line) compared to the distribution for *XMM*-COSMOS (red solid line). The distribution of sources common to both samples (black short dashed line) and the distribution of sources with available spectroscopic redshifts (see more details in Section 4) are also indicated (dotted and long dashed lines).

Here we present the photo-z of the 1692 sources for which a large number ($15 \geqslant N_{\rm filters} \leqslant 31$) of reliable photometric data are available. Note that 1677 of these sources have an optical counterpart in the updated, publicly available photometric catalog down to $i^*_{AB} = 26.5$ mag.[35]

[35] http://irsa.ipac.caltech.edu/data/COSMOS/tables/photometry/. This catalog includes the photometry in all the 25 optical/NIR broad-, intermediate-, and narrowband filters, from "u" to "K_s." The photometry is computed at the position of the i^*-band image, using Sextractor (Bertin & Arnouts 1996) in dual mode. The catalog supersedes that of Capak et al. (2007), with improved source detection and photometry extracted in 3″ apertures.

An additional 15 objects were found in the K-band catalog (McCracken et al. 2010) and aperture photometry were extracted in all broadband optical/near-IR and COSMOS bands using the K-band images as reference. We note that 11 of these 15 sources are also clearly visible in the optical images but are not present in the updated optical catalog because they are either close to a saturated source or below the detection limit.

For these 1692 sources, a coordinate cross-match (up to 0.″5) was performed between the optical catalog and the *Spitzer*/IRAC (Sanders et al. 2007) and *Galaxy Evolution Explorer* (*GALEX*; Zamojski et al. 2007) catalogs. To create the *GALEX* catalog, the U-band image was used as a prior, via point-spread function (PSF) fitting. Thus, the risk of wrong optical/UV identification is much lower. The IRAC images are deep ($[3.6\ \nu m]_{\rm AB}$ ∼24 mag) but they have large PSF. We performed simulations, which have shown that not more that 10% of the photometry of the ∼400,000 sources of the IRAC catalog may be effected by blending. This does not affect the associations optical/IRAC as we visually inspected the associations (Brusa et al. 2010; F. Civano et al. 2011, in preparation). However, the blending can affect the photometry of few sources, explaining the origin of a small number of outliers (see also a discussion in S09).

An additional 19 sources are neither detected in our optical images nor listed in the K-band catalog, but have a clear counterpart in the 3.6 μm images. Although these sources are potentially at high redshift, we do not attempt to estimate their photo-z as they have the same properties as the sources presented in Section 5.3 of S09 (in nine cases they are actually the same sources). There, the formal best-fit redshift was shown to be higher than four, but the redshift probability distribution function (PDFz) indicated that there were insufficient constraints to reject a solution at lower redshift. For these sources, only deeper photometry could provide reliable constraints and photo-z.

3. MORPHOLOGICAL AND VARIABILITY ANALYSIS

In S09, the optical counterparts of the *XMM* sources (presented in Brusa et al. 2010) were divided into two subsamples depending on their morphological and temporal properties. Objects that appeared as point sources (as defined in Leauthaud et al. 2007) in deep COSMOS *Hubble Space Telescope* (*HST*)/Advanced Camera for Surveys (ACS) images (Koekemoer et al. 2007) and/or showed brightness fluctuations were grouped as *QSOV* (short for point-like or varying) and their photometry was corrected for variability, if necessary. For this purpose, we introduced a parameter, VAR (Equation (1) in S09), which describes the deviation of the optical photometry from a reference epoch (2006, the time of quasi-simultaneous optical and *Spitzer*/IRAC observations). On the basis of the distribution of this parameter for the entire *XMM*-COSMOS sample, the photometry for the sources with VAR $>$ 0.25 mag were corrected. The threshold was chosen as the value of VAR at which the sample of extended sources in *XMM* displayed a sharp decline distribution (Figure 1 in S09). Sources that were not grouped in the *QSOV* sample were then classified as extended and non-varying (VAR $<$ 0.25) and were assigned to the *EXTNV* group. The identification of these two subgroups permitted us to use a luminosity prior that is typical of AGNs for the *QSOV* sample (see Section 4.3), which in turn reduced the parameter space of the possible photo-z solutions and thus the degeneracies.

The C-COSMOS sample discussed in the following was treated in an identical manner, and its VAR distribution is shown

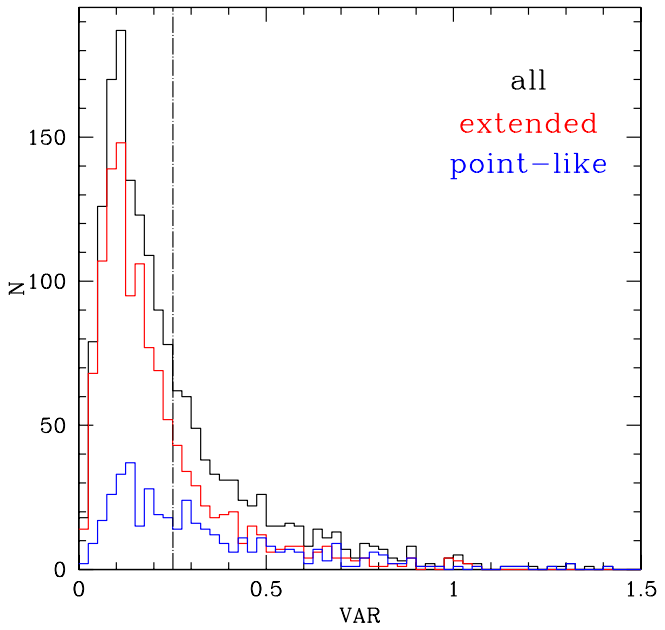

Figure 2. VAR histogram distribution for extended and point-like sources. As for *XMM*-COSMOS, we adopted the value VAR = 0.25 as a threshold beyond which we correct the photometry for variability.

in Figure 2. Compared to the *XMM*-COSMOS sample, the VAR distribution does not show a drop at VAR = 0.25 mag. This is expected, due to the deeper observations of the smaller area of C-COSMOS. However, we decided to adopt the same value in order to limit the number of caveats as much as possible and allow a more general procedure to be adopted.

We find that 766 sources satisfy the criteria for the *QSOV* sample, while 926 are classified as *EXTNV* sources. Among the *QSOV* sources, 442 (58%) were already included in the *XMM* sample, while the *EXTNV* sample contains 421 sources (46%), which were also detected with *XMM*.

4. PHOTOMETRIC REDSHIFT

In the following subsections, we describe the photo-z technique used for the C-COSMOS sources. As in S09, we used the publicly available *Le Phare* code[36] (Arnouts et al. 1999; Ilbert et al. 2006), which is based on a χ^2 template-fitting procedure. The templates that we used were either used for computing the photo-z for normal galaxies in Ilbert et al (2009, hereafter I09), or used for computing the photo-z for *XMM*-COSMOS in S09. The I09 templates include elliptical and spiral galaxy templates from Polletta et al. (2007). They also include blue star-forming galaxies generated with Bruzual & Charlot (2003). The S09 templates include some of the AGN library from Polletta et al. (2007), and hybrid templates combining AGNs and normal galaxies. How we created the templates, how we settled on the libraries, and how they compare with other libraries are widely described in I09 and S09, respectively. Extinction is added to the templates as a free parameter in the fit. We used the Calzetti et al. (2000) and the Prevot et al. (1984) attenuation laws. We also calibrated the zero points of the photometric catalog using the spectroscopic redshift sample of normal galaxies, as described in Ilbert et al. (2006) and I09. We did not allow any galaxy to be brighter than $M_B = -24$. For AGNs, the luminosity prior is more complex and depends on the classification *EXTNV*/*QSOV* (see Section 4.1). Finally, the full redshift probability distribution function is also derived.

After estimating the photo-z, we assessed the accuracy by comparing our results with 712 (21) reliable spectroscopic redshifts of galaxies (stars).

The spectroscopic redshifts were either publicly available via Sloan Digital Sky Survey Data Release 8 (SDSS DR8) or obtained within the COSMOS collaboration. In fact, the counterpart of X-ray targets was the primary targets of Magellan/IMACS (Trump et al. 2007) and MMT (Prescott et al. 2006) campaigns, or secondary targets in the zCOSMOS and zCOSMOS-deep surveys at Very Large Telescope (VLT)/VIMOS (Lilly et al. 2007, 2009; S. J. Lilly et al. 2011, in preparation), or again obtained at Keck/DEIMOS (PIs: Scoville, Capak, Salvato, Sanders, and Kartaltepe) and FLWO/FAST (Wright et al. 2010), respectively. While the spectroscopic sample used for the training for *XMM*-COSMOS reached a luminosity of $i^*_{AB} = 22.5$ mag, the new sample reaches magnitudes of $i^*_{AB} = 25.4$ mag($\langle i^*_{AB} \rangle = 21.3$ mag; vertical dot-dashed line in Figure 1), thus providing some insight into the faint source population. Note that *all* the spectroscopic redshifts have a probability higher than 75% of being secure, as at least two emission/absorption features were used for the redshift determination.

Throughout the paper, we measure the accuracy of the photo-z using the normalized median absolute deviation (NMAD; Hoaglin et al. 1983) defined as $\sigma_{NMAD} = 1.48 \times \mathrm{median}(|z_{phot} - z_{spec}|/(1 + z_{spec}))$. For a Gaussian distribution, σ_{NMAD} is directly comparable to the definition adopted in other papers that directly quote $\sigma_{\Delta z/(1+z_{spec})}$. This dispersion estimate is relatively insensitive to catastrophic outliers (i.e., objects with $|z_{phot} - z_{spec}|/(1 + z_{spec}) > 0.15$). The fraction of outliers is denoted by η. After applying a method identical to that used for the *XMM* sample, we discuss how to improve the reliability of photo-z for the *EXTNV* and *QSOV* subsamples, respectively.

4.1. Estimating C-COSMOS Photo-z as for XMM-COSMOS

To understand whether or not C-COSMOS is sampling the same population as *XMM*-COSMOS sources, we first computed photo-z following the same procedure as described in detail in S09. In particular, after dividing the C-COSMOS sources into *EXTNV* and *QSOV*, we used the same template library, consisting mostly of AGNs and hybrid templates. The hybrid templates are constructed by combining galaxy and AGN empirical SEDs (details of the templates and their construction are fully described in S09). Furthermore, the same luminosity previously applied to the absolute B-band magnitude ($-20 > M_B > -30$) was adopted for the *QSOV* sample.

We compare the resulting photo-z with the spectroscopic sample of 712 sources. Note that the spectroscopic sample is a close approximation to a *blind* sample, different in its properties from the sample used as *training* of the photo-z for *XMM*-COSMOS. Indeed, only 273 of these sources were included in the original training sample used in S09. The new 439 sources had either no spectroscopy at that time or lie below the *XMM* flux limit.

While most of the photo-z are still excellent, the resulting fraction of outliers ($\eta = 9.0\%$) and accuracy ($\sigma_{NMAD} \sim 0.031$) do not reach the quality obtained for the *XMM*-COSMOS sample ($\eta = 5\%$, $\sigma_{NMAD} = 0.015$ for sources $i^*_{AB} < 24.5$ mag). In particular, if we consider only the C-COSMOS sources brighter than $i^*_{AB} < 22.5$ mag (limit of the spectroscopic training sample used in *XMM*-COSMOS), the accuracy for the *EXNV* and *QSOV*

[36] http://www.oamp.fr/people/arnouts/LE_PHARE.html.

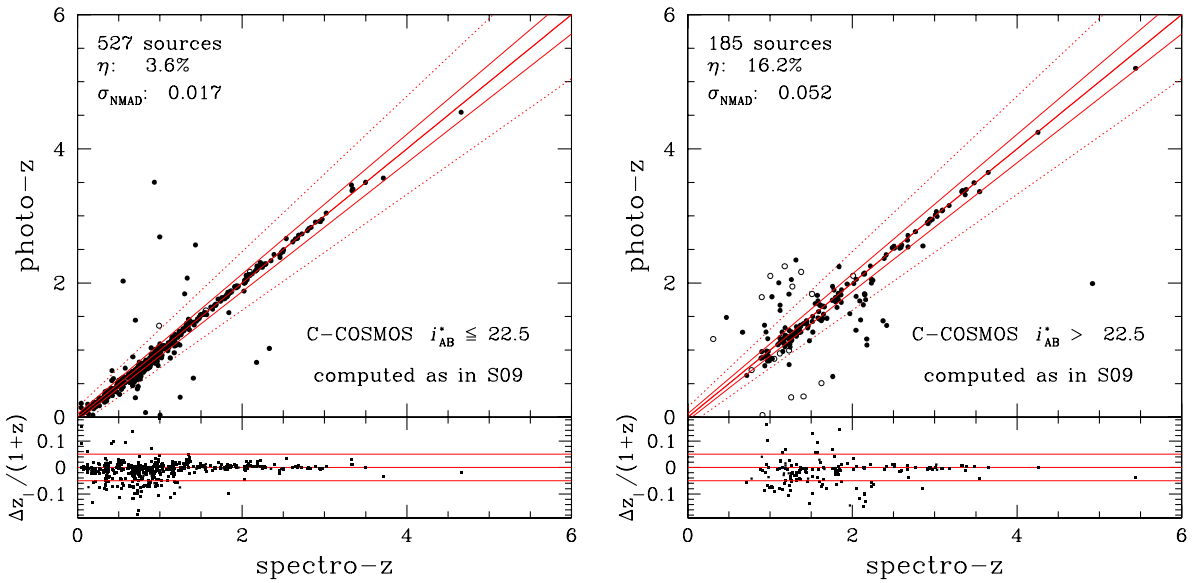

Figure 3. C-COSMOS photometric redshifts computed following the recipe defined in S09, compared to the spectroscopic redshifts. The comparison is shown for sources brighter (left panel) and fainter (right panel) than $i^*_{AB} = 22.5$ mag. Open circles represent sources for which there is at least a second significant peak in the redshift probability distribution. The solid lines correspond to $z_{phot} = z_{spec}$ and $z_{phot} = \pm 0.05(1 + z_{spec})$, respectively. The dotted lines limit the locus where $z_{phot} = \pm 0.15(1 + z_{spec})$. While the quality of the photo-z for the bright sample is comparable to that obtained for the *XMM*-COSMOS sources without any new tuning or training, the photo-z computed for the fainter sources are significantly worse in terms of both the dispersion and fraction of outliers.

(A color version of this figure is available in the online journal.)

subsamples is the same as for *XMM*-COSMOS, even if the spectroscopic sample used for the comparison is not the same. In contrast, for sources fainter than $i^*_{AB} = 22.5$ mag, we found a significant increase in the fraction of outliers, and lower accuracy (compare Figure 3 of this paper with Figures 4 and 12 in S09) is obtained.

The comparable quality of the photo-z between C-COSMOS and *XMM*-COSMOS at $i^*_{AB} < 22.5$ mag suggests that the optically bright populations probed by *XMM* and *Chandra* are similar and that the template library used in S09 is largely representative of their properties. In S09, there was no spectroscopic training sample for $i^*_{AB} > 22.5$ mag and the quality assessment for faint sources ($i^*_{AB} > 22.5$ mag) was based on the comparison with only 46 spectroscopic redshifts. The faint C-COSMOS spectroscopic sample now includes a total of 185 sources with $i^*_{AB} > 22.5$ mag and the lower photo-z quality may indicate that a new treatment, different from that used for the bright sample, is required.

4.2. Revised Treatment for the C-COSMOS EXTNV Sample

Twenty-four out of the 30 templates used to compute the photo-z for the *XMM*-COSMOS sources are dominated (from the 10% to 100% level) by an AGN component. On the other hand, as C-COSMOS extends to faint X-ray sources and thus also to faint and potentially optically obscured sources, one could argue that the library used to analyze the *XMM* data is not fully representative. It might be beneficial to consider a library including a set of "pure galaxy" templates. This is particularly true for the *EXTNV* subsample, which contains predominantly nearby sources where the optical/near-IR emission is expected to be dominated by the host galaxy light.

To assess the impact of a different library of templates, we computed the photo-z using the library and settings defined in I09. These authors used a library of 31 templates of normal galaxies to compute the photo-z of two million normal galaxies ($i^*_{AB} < 26.5$) in the entire COSMOS field, reaching an accuracy of $\sigma_{NMAD} \sim 0.015$ with a fraction of outliers $\eta < 5\%$. In particular, the authors included emission lines in the templates, as they were shown to contribute to various colors by up to 0.4 mag.

In Table 1, we compare the resulting quality of the photo-z for bright ($i^*_{AB} < 22.5$) and faint ($i^*_{AB} > 22.5$) *EXTNV* subsamples with the results obtained using the S09 library.

From the comparison of the dispersions obtained in the bright, faint, and full optical ranges, it seems that a library of normal galaxies generally works better for the *EXTNV* sample than a library which includes AGN templates. However, for the bright sample, the fraction of outliers obtained when using the library of normal galaxies is almost twice that obtained using the library of AGN-dominated templates, indicating the need for the former library for at least some sources. In addition, the result is consistent with that found for the sources in *XMM*-COSMOS, after recomputing the photo-z now also using the H-band photometry (last columns of Table 1).

To characterize the outliers and see whether they depend on the properties of the sources, we plot in the left panel of Figure 4 all the *EXTNV* sources as a function of their soft X-ray flux and their X/O ratio (Maccacaro et al. 1988). In this specific case, using the soft X-ray flux and the optical i^* AB magnitude, the X/O ratio is defined as $\log(F_X/F_{opt}) = \log(F_{(0.5-2\,keV)}) + 5.57 + i^*$ [AB]/2.5. The ratio can be used as a first-order assessment of the nature of a source, with a galaxy being characterized by X/O < -1.5 and an AGN-dominated source by $-1 <$ X/O < 1.

Both libraries are clearly able to reproduce the spectroscopic sample of galaxy-dominated sources because in the range X/O < -1.5 there are virtually no outliers. In addition, within the locus of AGN-dominated sources, the distribution of outliers when using either library (red open circles and yellow filled circles for I09 and S09, respectively) is independent of the X/O ratio. The only real difference is visible in the distribution of outliers as a function of X-ray flux, where the library of AGN-dominated templates provides more reliable photo-z at high X-ray fluxes, with only two outliers above

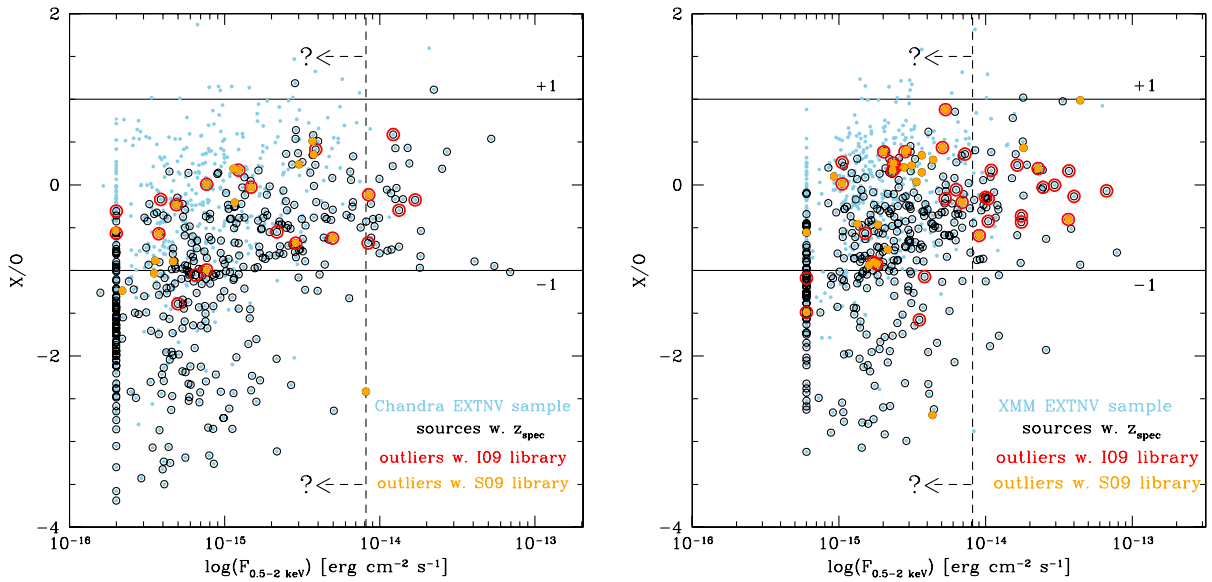

Figure 4. Distribution of outliers for the *EXTNV* samples (left: C-COSMOS; right: *XMM*-COSMOS) as a function of X/O and soft X-ray flux and compared to the rest of the sources distribution. Light blue dots represent all the sources, while black circles represent sources with spectroscopic redshift. Red circles indicate outliers for the library of normal galaxies of I09, while yellow filled circles indicate the outliers for the AGN-dominated S09 library. The distribution of outliers is the same along the X/O axis. However, for each library, the outlier fraction depends on the X-ray flux of the source. While there is an excess of outliers at bright X-ray fluxes for normal galaxy templates, the inverse occurs for the library of AGN-dominated templates at the faint end of X-ray fluxes.

Table 1
Assessing Quality of Photo-z for the *EXTNV* Subsamples Using Different Libraries

	C-COSMOS *EXTNV*						*XMM*-COSMOS *EXTNV*	
	$i < 22.5$		$i > 22.5$		All		$i < 22.5$	
Library	η (%)	$\sigma_{\rm NMAD}$	η (%)	$\sigma_{\rm NMAD}$	η (%)	$\sigma_{\rm NMAD}$	η (%)	$\sigma_{\rm NMAD}$
I09[a]	4.2	0.015	9.0	0.041	5.7	0.017	7.7	0.017
S09[b]	2.7	0.020	18.4	0.083	6.0	0.028	4.4	0.022
Combined[c]	2.4	0.014	10.3	0.041	4.1	0.017	4.7	0.016

Notes.
[a] Library from I09; only normal galaxy templates.
[b] Library from S09; mostly AGN-dominated templates.
[c] Final result obtained using the I09 or S09 library, depending on the X-ray flux of the sources.

$F_{(0.5-2\,\rm keV)} > 8 \times 10^{-15}\,\rm erg\,cm^{-2}\,s^{-1}$ in contrast to the five for the library of normal galaxies. This is consistent with the fact that the extended, optically bright, and X-ray bright sources in our sample are nearby ($z < 1$) Seyfert galaxies or QSOs. Indeed, all the sources with spectroscopic redshift and with $F_{(0.5-2\,\rm keV)} > 8 \times 10^{-15}\,\rm erg\,cm^{-2}\,s^{-1}$ have an absolute B magnitude $M_{\rm B} < -20$, which is typical for AGNs (e.g., Veron-Cetty & Veron 2001). In contrast, fainter X-ray sources are either host-dominated or low luminosity or obscured AGNs for which the templates of normal galaxies are able to mimic the SED, thus correctly reproducing the redshift.

On the basis of the available spectroscopic sample (open black circles), we argue that adopting a threshold at $F_{(0.5-2\,\rm keV)} > 8 \times 10^{-15}\,\rm erg\,cm^{-2}\,s^{-1}$ and using the library of either normal galaxies or AGN-dominated templates for sources, respectively, below or above this value, improves the accuracy of the photo-z, as demonstrated in the last row of Table 1 (indicated as "combined").

Given the small number of outliers in the bright end of the X-ray flux, one could argue that the introduction of different templates depending on the X-ray flux is unnecessary and that for the *EXTNV* the library of normal galaxies could be used by default. However, for wide-field shallower X-ray surveys such as *XMM*-COSMOS, where a large number of bright X-ray sources are detected, the use of AGN-dominated templates in the library is more important (see the right panel of Figure 4). This new approach allows us to reduce the fraction of outliers at any X-ray flux and, at the same time, reduces the dispersion, which is now symmetric and peaks at $\Delta z/(1 + z_{\rm spec}) = 0$ (compare yellow and black histograms in Figure 5 for C-COSMOS and *XMM*-COSMOS, respectively).

We note that the adopted X-ray threshold is chosen to minimize the number of outliers and thus it strongly depends on the spectroscopic sample available for the comparison. The value is, at the moment, fixed where the first outlier for the AGN-dominated library appears in the C-COSMOS *EXTNV* sample, but could possibly be moved to fainter X-ray fluxes, depending on the availability of future spectroscopy in the range $F_{0.5-2\,\rm keV} = 4$–$8 \times 10^{-15}\,\rm erg\,cm^{-2}\,s^{-1}$.

4.3. Analysis of the QSOV Sample

As for the C-COSMOS *EXTNV* sample, the photo-z accuracy of C-COSMOS *QSOV* sources is identical to that achieved for *XMM QSOV* sources when the analysis is limited to sources brighter than $i^*_{\rm AB} = 22.5$ mag ($\sigma_{\rm NMAD} = 0.011$ and $\eta = 5.1\%$). However, the fraction of outliers increases to $\eta = 14.3\%$

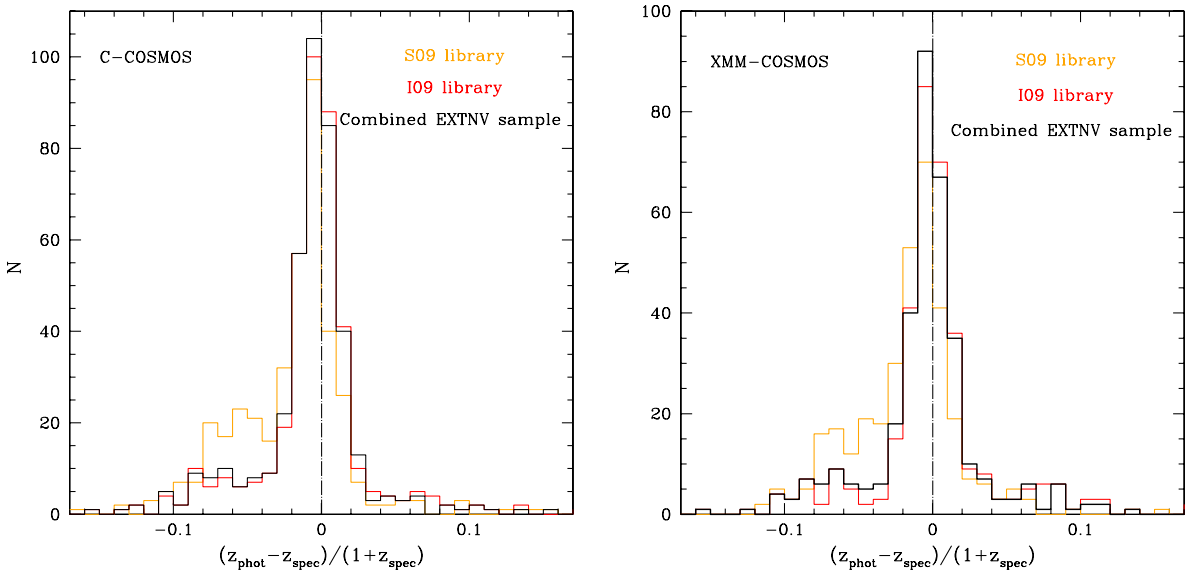

Figure 5. Left: $\Delta z/(1+z_{\rm spec})$ distribution for the C-COSMOS *EXTNV* subsample using the I09 library of normal galaxies (red solid line), and the S09 library of AGNs (yellow solid line). The black solid line indicates the final result using S09 for $F_{0.5-2\,\rm keV} < 8\times10^{-15}$ erg cm^{-2} s^{-1} and I09 for fainter sources. Right: the same but for the *XMM*-COSMOS sample.

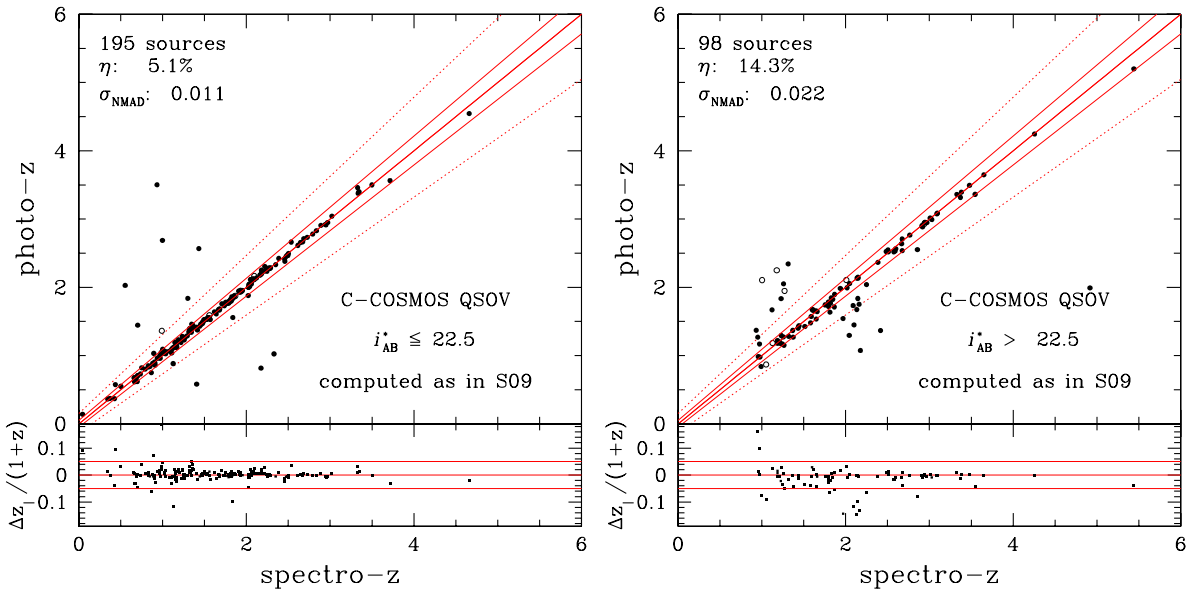

Figure 6. Comparison between spectroscopic and photo-z computed as in S09 for the C-COSMOS *QSOV* sources, brighter (left panel) and fainter (right panel) than $i^*_{\rm AB} = 22.5$. Black open circles indicate sources with a second possible solution in the redshift probability distribution. Again, the quality of the photo-z for the bright sample is comparable to that obtained for the *XMM*-COSMOS *QSOV* sources without any additional tuning, even if the spectroscopic training sample is different.

(consequently, $\sigma_{\rm NMAD} = 0.22$) if we limit the analysis only to the 98 sources fainter than $i^*_{\rm AB} = 22.5$ mag. We indeed find that ∼60% of the outliers in the *QSOV* sample are represented by faint sources (Figure 6) and that they are concentrated in two redshift ranges, where the photo-z are systematically overestimated ($1 < z_{\rm spec} < 1.5$) or underestimated ($2 < z_{\rm spec} < 2.5$) relative to the spectroscopic redshifts.

In an attempt to understand the origin of the systematic errors, as in the previous section, we plot in Figure 7 the outliers obtained using the S09 library (yellow filled circles) as a function of optical and X-ray brightness. For the sake of completeness, we also plot the outliers that are obtained by using the library of normal galaxies from I09 (red circles), imposing this time the luminosity prior $-20 < M_{\rm B} < -30$. We demonstrated in S09 that this library is unsuitable for the *XMM QSOV* sample, but in Table 2 and Figure 7 this can be seen more clearly. For the *QSOV* sample, the library of AGN templates helps to measure more accurate photo-z than the library of normal galaxies at any X-ray flux and any optical magnitude.

Table 2
Results for the C-COSMOS *QSOV* Sample Using S09 and I09 Libraries

Library	*QSOV*, i^* <= 22.5		*QSOV*, i^* > 22.5		*EXTNV*, all	
	η (%)	$\sigma_{\rm NMAD}$	η (%)	$\sigma_{\rm NMAD}$	η (%)	$\sigma_{\rm NMAD}$
I09	45.6	0.165	23.5	0.074	38.2	0.135
S09	5.1	0.011	14.3	0.022	8.2	0.013

Thus, the main limitation to the accuracy of the photo-z and the fraction of outliers appears to be related to the optical faintness of the sources. As already pointed out by other authors (e.g., Cardamone et al. 2010; Barro et al. 2011), at

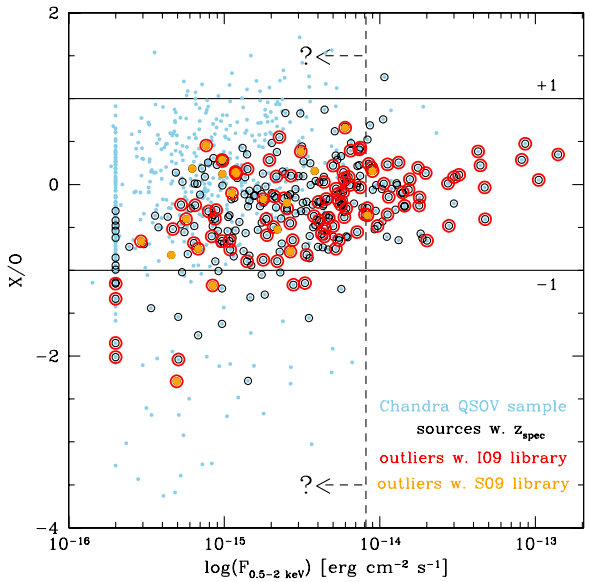

Figure 7. Same as in Figure 4 but for the C-COSMOS *QSOV* sample. Clearly, the templates for normal galaxies are unsuitable for this sample.

fainter magnitudes the spectral energy distribution is less tightly constrained, and only by upper limits in some bands, or has large statistical uncertainties associated with the photometry. Thus, the 1σ error associated with $z_{\rm phot}$ steadily increases with the i^*-band magnitude for the COSMOS multi-wavelength data set (see S09; I09). Only deeper photometry in near-IR (NIR) bands (where the 4000 Å break falls $2 < z < 2.5$) will allow us to improve the accuracy of the photo-z for the faint sources in the C-COSMOS and *XMM*-COSMOS *QSOV* samples. Thus, an opportunity to improve the results for at least a fraction of the sources will be given with the photometry from the ULTRAVISTA survey[37] and the future observations taken with *HST*/WFC3 by the CANDELS survey (Grogin et al. 2011; Koekemoer et al. 2011).

5. RESULTS

In summary, using the procedure described in the paper and illustrated in the flow-chart of Figure 8, we obtained high-quality photo-z for C-COSMOS. In addition, we recomputed the photo-z of *XMM*-COSMOS sources for which the H-band photometry is now available. For both samples (see Figure 9), we obtained an accuracy of $\sigma_{\rm NMAD} = 0.015$ and a similar fraction of outliers $\eta \sim 6\%$. The addition of the H-band photometry and our revised strategy for treating the extended, optically non-varying, faint X-ray sources in the *EXTNV XMM*-COSMOS sample resulted in a change in photo-z of $\Delta z > 0.2$ for 248 sources ($\sim$15% of the total *XMM*-COSMOS sample). This improved accuracy with respect to the old version of the photo-z catalog (Salvato et al. 2009) is summarized in Table 3. It is reassuring that the introduction of the H-band photometry does not affect the accuracy of the *QSOV* sample, illustrating the reliability of our photo-z in the field.

The final photo-z catalogs for the C-COSMOS and *XMM*-COSMOS surveys are available[38] in ASCII format, together with morphological and variability analysis. Excerpts of the catalogs are provided in Tables 4 and 5.

[37] http://www.strw.leidenuniv.nl/~ultravista/.
[38] http://www.ipp.mpg.de/~msalv/PHOTOZ_XCOSMOS/.

In both catalogs, we flagged as *stars* those sources that are point-like and have $1.5 \times \chi^2_{\rm star} < \chi^2_{\rm agn/gal}$, where $\chi^2_{\rm star}$ and $\chi^2_{\rm agn/gal}$ are the reduced χ^2 for the best-fit solutions obtained with stellar and AGN or galaxy libraries. For C-COSMOS (*XMM*-COSMOS), we found 33 (53) candidate stars, 18 (32) of which are already spectroscopically confirmed. The criterion fails to identify 5 (3) sources that are known to be stars via spectroscopy. A more relaxed criterion, such as the one used in I09 and S09 (point-like and $\chi^2_{\rm star} < \chi^2_{\rm agn/gal}$), would allow the identification of all the spectroscopic stars, but would also misclassify as star objects those that are spectroscopically confirmed galaxies.

The redshift distribution for the galaxies in the two samples (red: C-COSMOS; blue: *XMM*-COSMOS) is shown in Figure 10, where the histograms are normalized to the respective total number of sources. As expected, the deeper X-ray observations of C-COSMOS allowed us to detect sources at higher redshift (from $z \sim 1.8$) than *XMM*-COSMOS.

To assess any other differences in the populations of the two surveys, we considered the C-COSMOS sources that are respectively below (C-COSMOS faint) and above (C-COSMOS bright) the flux limit of *XMM*-COSMOS ($F_{0.5-2\,\rm keV} = 10^{-15}$ erg cm^{-2} s^{-1}). The comparison between the two subsamples and the *XMM*-COSMOS survey is shown in Figure 11, where the black solid line represents the redshift distribution of the C-COSMOS faint sources and the thick-dashed and thin-dotted black lines represent C-COSMOS bright and *XMM*-COSMOS sources, respectively. While C-COSMOS bright and *XMM*-COSMOS do not differ, the Kolmogorov–Smirnov (K-S) test suggests that the population of sources in the C-COSMOS bright and faint is not extracted from the same parent population ($P_{\rm H_0} \sim 0.006\%$), as already appeared to be clear from Figure 10.

In our additional analysis, we divided the samples according to the best-fit SED template. Red lines trace the cumulative distributions of the sources fitted by normal galaxy templates, while green and blue lines indicate sources that can be most accurately described by type 2 AGN and type 1 AGN templates, as defined in S09. The K-S test gives a probability of $P_{\rm H_0} \sim 0.001$, $P_{\rm H_0} \sim 0.014$, and $P_{\rm H_0} \sim 0.011$ that the three populations (galaxies, type 1, and type 2 AGNs) are drawn from the same population for C-COSMOS and *XMM*-COSMOS. This is somehow implicit in the procedure used to estimate the photo-z, as we change our library in accordance with the X-ray flux for the *EXTNV* samples and C-COSMOS being deeper than *XMM*. We fitted 90% and 95% of the *EXTNV* C- and *XMM*-COSMOS sources, respectively, using the library of normal galaxies.

However, we note that even if these sources are more accurately described by normal galaxy templates, they are not normal galaxies. We can more accurately describe 994 (935) of the 1098 (1045) C-COSMOS (*XMM*-COSMOS) sources ($\sim$91%) using a normal galaxy template, but these sources have X-ray luminosities above 10^{42} erg s^{-1} and thus can be assumed to be powered by an active nucleus.

5.1. The Highest Redshift X-Ray-selected Sources?

By combining their spectroscopic and photometric data, Civano et al. (2011) presented the log$N$–log$S$ and space density of C-COSMOS high-z sources ($z > 3$), and we refer to this paper for a detailed discussion of the high-z X-ray source population. Here, we present the photometric properties of the highest-z X-ray-selected candidate AGNs and investigate the effects of different assumptions about the SED templates and luminosity priors on the photo-z estimation, and its stability and reliability.

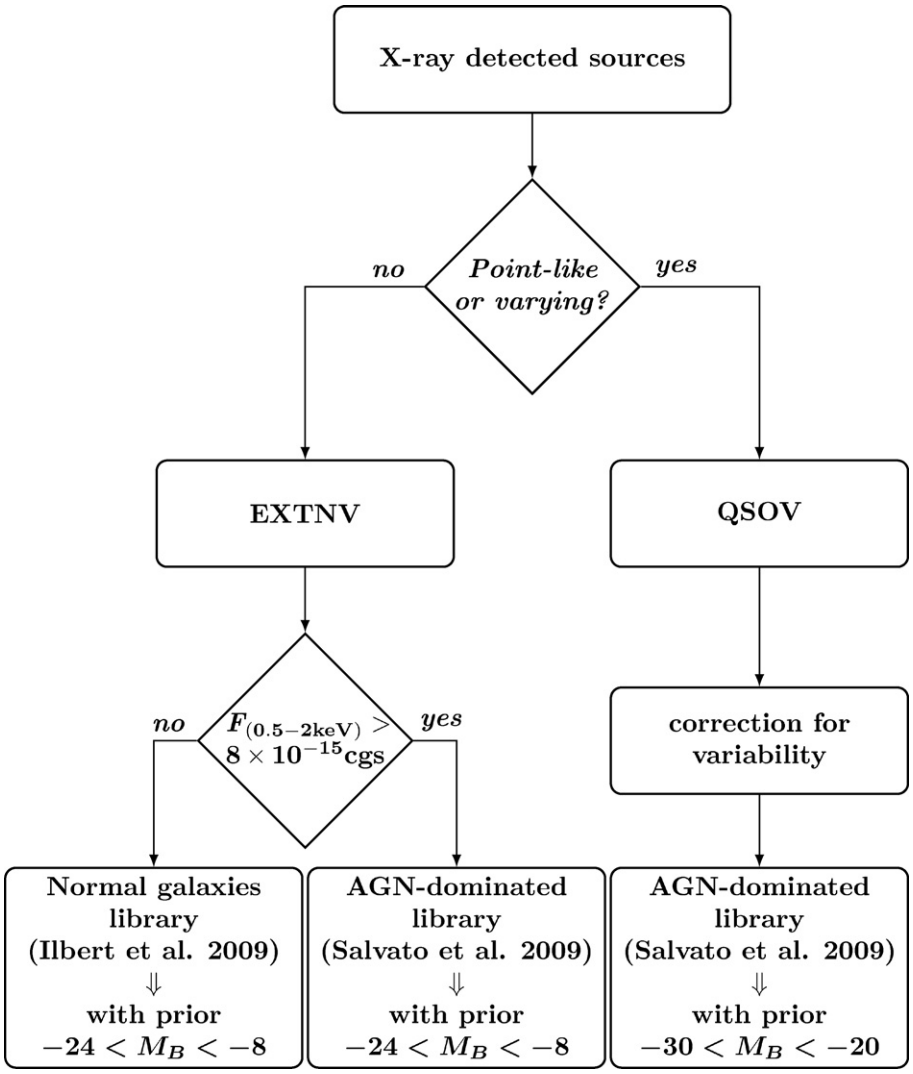

Figure 8. Flow chart of the procedure adopted to compute photo-z for X-ray-detected sources.

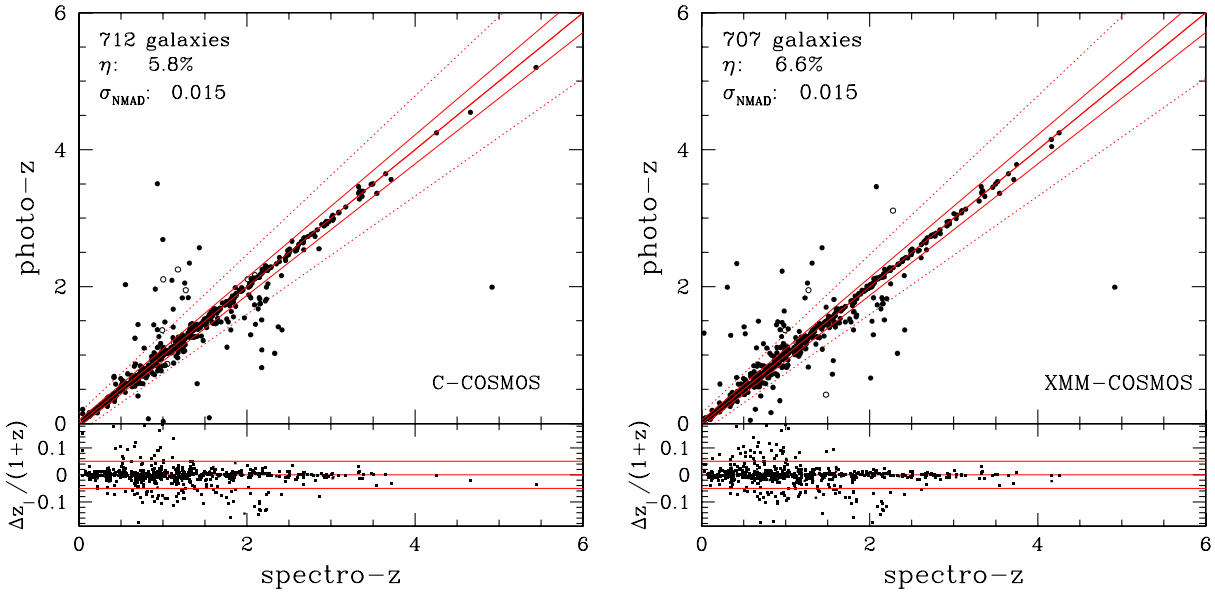

Figure 9. Final photometric vs. spectroscopic redshifts for the entire C-COSMOS (left) and *XMM*-COSMOS (right) samples.
(A color version of this figure is available in the online journal.)

Table 3
XMM-COSMOS Recomputed

	$i^* < 22.5$						Total		
	EXTNV			*QSOV*			*QSOV+ EXTNV*		
Library	N^a	η	σ_{NMAD}	N^a	η	σ_{NMAD}	N^a	η	σ_{NMAD}
Results from S09	218	2.3%	0.019	178	6.3%	0.012	442	5.3%	0.017
Same procedure as S09 with addition of *H*-band and more spectroscopy	270	4.4%	0.022	236	7.2%	0.013	590	6.3%	0.017
New method	270	4.1%	0.017	236	7.2%	0.013	590	6.1%	0.015

Note. [a] Number of sources with spectroscopic redshift.

Table 4
Extracted from the C-COSMOS Photometric Redshift Catalog

XID (1)	ID (Ilbert) (2)	z_{phot} (3)	z_{phot}lower (4)	z_{phot}upper (5)	PDFz (6)	Template (7)	Morphology (8)	VAR (9)
1	860777	1.93	1.86	2.03	86.52	3	−999	0.48
6	1081059	1.12	1.11	1.14	100.00	1	1	0.83
14	1046901	2.15	2.07	2.21	95.67	22	1	0.30
21	1007423	1.86	1.85	1.88	100.00	30	2	0.28
23	997226	2.93	2.91	2.95	67.41	1	1	0.44
25	974083	1.99	1.95	2.04	98.81	5	−999	0.31
26	969546	0.73	0.72	0.74	100.00	28	2	0.57
27	974555	1.51	1.46	1.57	95.59	5	1	0.47
29	972975	1.08	1.05	1.10	99.76	20	2	0.17
31	978155	2.62	2.6	2.62	100.00	26	2	0.06

Notes. Excerpt from the photo-z catalog available online for C-COSMOS. Column 1: F. Civano et al. (2011, in preparation) identifier; Column 2: optical identifier number as reported in the optical catalog and in Ilbert et al. (2009); Column 3: photometric redshift; Columns 4 and 5: lower and upper values of photometric redshift; Column 6: redshift probability distribution; Column 7: best-fit template—from 1 to 30 the templates are from S09, templates from 100+(1–31) are from the I09 library; Column 8: morphological classification (from Leauthaud et al. 2007)—1 or 3 indicates extended sources, while 2 or 4 indicates point-like sources; Column 9: variability. A revised photo-z catalog for *XMM*-COSMOS, with the same structure, is available at the same address.

(This table is available in its entirety in a machine-readable form in the online journal. A portion is shown here for guidance regarding its form and content.)

Table 5
Extracted from the *XMM*-COSMOS Photometric Redshift Catalog

XID (1)	ID (Ilbert) (2)	z_{phot} (3)	z_{phot}lower (4)	z_{phot}upper (5)	PDFz (6)	Template (7)	Morphology (8)	VAR (9)
1	786683	0.372	0.360	0.380	100.000	28	2	0.18
2	1054439	1.043	1.030	1.050	100.000	30	2	0.20
3	1290981	0.364	0.350	0.370	100.000	29	2	0.34
5	1063264	1.181	1.170	1.190	100.000	30	2	0.34
7	1418792	1.311	1.300	1.320	100.000	6	1	0.26
8	1472056	0.702	0.690	0.710	100.000	26	2	0.08
9	1265494	1.465	1.450	1.480	100.000	30	2	0.21
10	1032058	0.682	0.670	0.690	100.000	22	2	0.14
11	777509	1.209	1.200	1.220	100.000	27	2	0.36
12	771981	1.272	1.260	1.290	100.000	27	2	0.05

Notes. Excerpt from the photo-z catalog available online for *XMM*. Column 1: *XMM* identifier (from Brusa et al. 2010); Column 2: optical identifier number as reported in the optical catalog and in Ilbert et al. (2009); Column 3: photometric redshift; Columns 4 and 5: lower and upper values of photometric redshift; Column 6: redshift probability distribution; Column 7: best-fit template—from 1 to 30 the templates are from S09, templates from 100+(1–31) are from the I09 library; Column 8: morphological classification (from Leauthaud et al. 2007)—1 or 3 indicates extended sources, while 2 or 4 indicates point-like sources; Column 9: variability. A revised photo-z catalog for *XMM*-COSMOS, with the same structure, is available at the same address.

(This table is available in its entirety in a machine-readable form in the online journal. A portion is shown here for guidance regarding its form and content.)

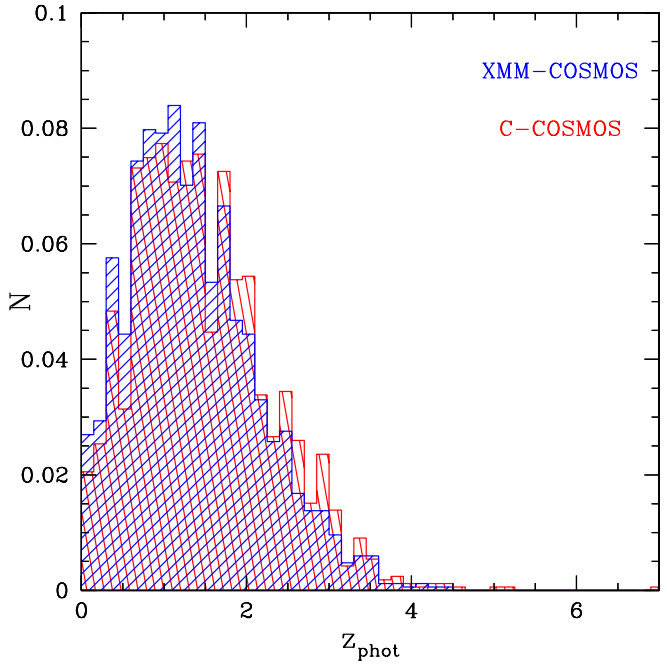

Figure 10. Photo-z distribution for C-COSMOS (red) and *XMM*-COSMOS (blue), normalized to the respective total number of sources.

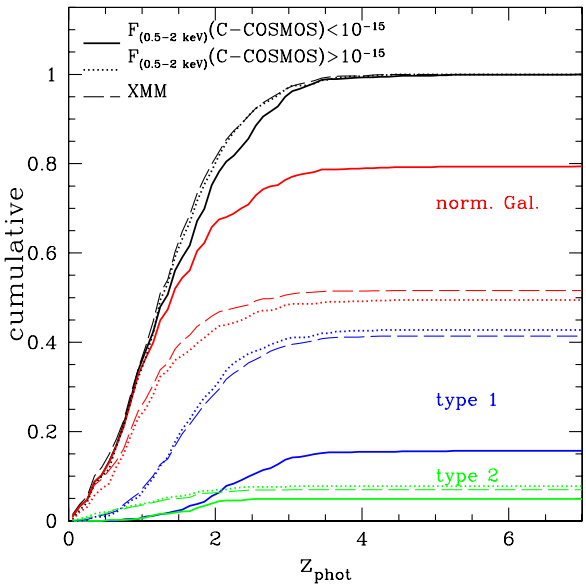

Figure 11. Normalized, cumulative redshift distribution for all *XMM*-COSMOS sources (black dashed line) and C-COSMOS sources with soft X-ray flux below (black solid line) or above (black dotted line) the detection limit of *XMM*-COSMOS ($F_{0.5-2\,\mathrm{keV}} = 10^{-15}$ erg cm^{-2} s^{-1}). Red lines indicate the sources more accurately described by templates of normal galaxies, while blue and green lines indicate sources better fit by type 1 and type 2 AGNs, respectively.

High-redshift AGNs provide key observational constraints on the theoretical models of galaxy and supermassive black hole formation and evolution. Most models can describe the high-luminosity regime well up to $z \sim 2$–3 (Hopkins et al. 2008; Menci et al. 2008, and references therein). However, the shortage of observational data for both high-redshift and low-luminosity AGN populations has restricted the progress of the modeling. Since these predictions are generally applied to determine the key physical parameters such as the QSO duty cycle, the black hole seed mass function, and the accretion rates, reliable observations of the QSO luminosity function and its evolution at high redshift are required (F. Civano et al. 2011; Brusa et al. 2010; Aird et al. 2010; Fontanot et al. 2007).

In addition to the 19 sources that, as discussed in Section 2, are potentially at $z_{\mathrm{phot}} > 4$, the C-COSMOS sample contains a single source for which the most likely photo-z solution is at $z > 6$. In contrast to the typical results for high-z candidate sources, the PDFz is both peaked and narrow. The counterpart to the source CID-2550 is detected longward of 9000 Å ($z_{\mathrm{AB}} = 25.4$ mag, $J_{\mathrm{AB}} = 23.6$ mag, $H_{\mathrm{AB}} = 23.8$ mag, $K_{\mathrm{AB}} = 23.0$ mag, $[3.6\,\mu\mathrm{m}]_{\mathrm{AB}} = 22.8$ mag, $[4.5\,\mu\mathrm{m}]_{\mathrm{AB}} = 22.7$ mag, $[5.8\,\mu\mathrm{m}]_{\mathrm{AB}} = 21.7$ mag, $[8\,\mu\mathrm{m}]_{\mathrm{AB}} = 21.7$ mag; see left panel of Figure 12) and is also marginally seen in the deep Subaru i^+-band observations (≈26.6 mag).

Photo-z are usually very sensitive to luminosity priors, in particular when the available photometry has large uncertainties and/or the number of the photometric points are insufficiently large to reliably determine a photo-z. This is the case for CID-2550, where in the optical bands we have either an upper limit or errors larger than 1 mag. Imposing a lower limit to the absolute magnitude of $M_B = -20.5$ results in a unique (PDFz = 98%) solution at $z_{\mathrm{phot}} = 6.84$, with a best-fit SED solution being obtained using an AGN+ULIRG hybrid (QSO1+IRAS22491; see S09). Without any luminosity prior, the best-fit photo-z solution becomes $z_{\mathrm{phot}} = 6.94$ (PDFz = 85%) with a second, less probable solution at $z_{\mathrm{phot}} = 1.59$ (see Figure 12, where, in cyan, we also plot the best fit obtained with a library of stars). The template that most accurately describes the data remains the same, while for the low-redshift solution a dusty blue SB template from Bruzual & Charlot (2003) is preferred.

The high-redshift solution suggested by the PDFz is also supported by the very small number of outliers that we obtain at high redshift (only 1 out of 53 sources at $2.5 < z_{\mathrm{spec}} < 5.4$, with $\sigma_{\mathrm{NMAD}} = 0.009$). In addition, a solution at $z = 6.84$ would explain the marginal detection in the deep Subaru i^+ band as emission from Lyβ caused by an incomplete Gunn–Peterson trough (Becker et al. 2001; Fan et al. 2006). The source is also comparable to the Extreme X-ray/Optical ratio sources (EXOs) first defined by Koekemoer et al. (2004), which are selected as optical dropouts with X-ray emission, although the improved multi-wavelength data available here for CID-2550 provide a stronger photo-z solution.

At $z \sim 6.84$, the 0.5–7 keV X-ray luminosity for CID-2550 would be $\log(L_X) = 44.67$ erg s^{-1}, while the absolute B-band magnitude would be $M_B = -24.6$, i.e., a significantly high QSO luminosity. Assuming (1) that the quasar emits at the Eddington luminosity, (2) an X-ray bolometric correction in the range 10–100, and (3) that neither lensing nor beaming significantly magnifies the observed flux, we estimate a central black hole mass in the range $\approx 4 \times 10^{7-8}\,M_{\odot}$. This mass estimate is lower than the average mass derived for the sample of bright optically selected $z > 6$ quasars from SDSS (Fan et al. 2001; Willott et al. 2003), suggesting that X-ray selection might detect less extreme objects, or objects in a different, possibly obscured (as suggested by the best-fit hybrid galaxy template), phase of rapid growth.

6. DISCUSSION

6.1. Importance of Spectroscopic Sample

Most galaxy and AGN (co)evolutionary studies depend on photo-z estimates. Spectroscopy is extremely challenging, in particular, at high redshift, where photo-z then play a funda-

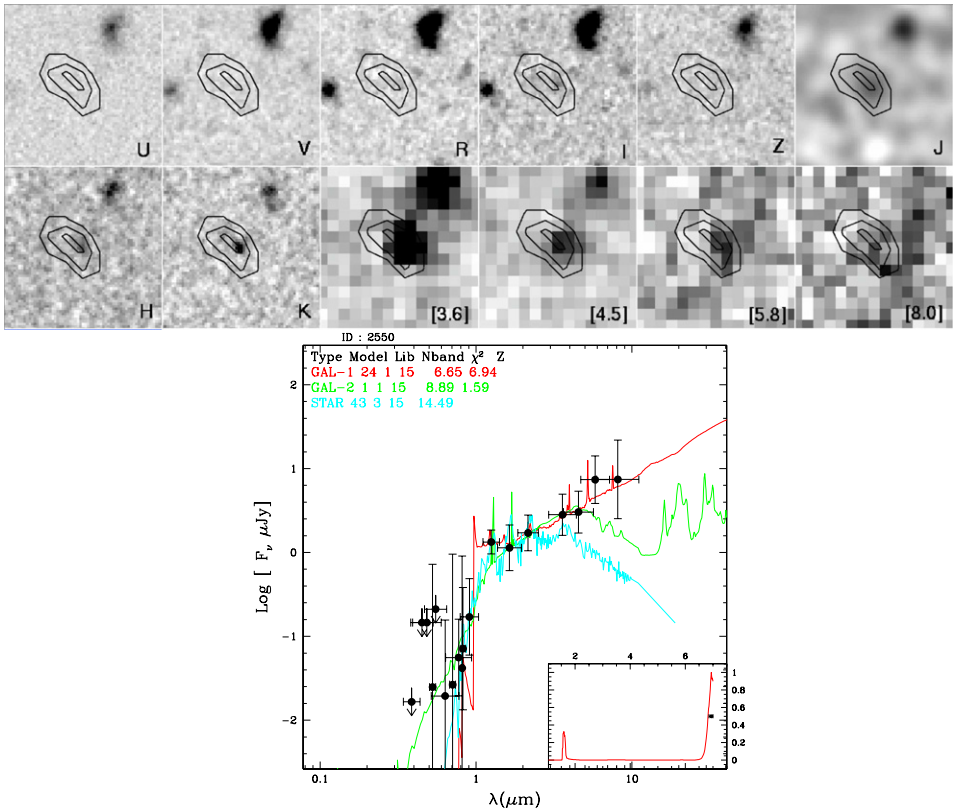

Figure 12. Left: from top left to bottom right, stamp images ($10'' \times 10''$) in U, V, R, I, Z, J, H, K, and the four IRAC channels (3.6, 4.5, 5.8, and 8 μm) for CID-2550. Black contours indicate the X-ray detection. The source is clearly visible in the bands redder than 9000 Å. Right: spectral energy distribution of source CID-2550. Depending on the adopted luminosity priors, one or two photo-z solutions are found, although the low-redshift solution always has very low PDFz.

mental role. The photo-z accuracy is usually estimated by comparing it with a small spectroscopic sample of bright and/or nearby objects. Both the telescope diameter and the wavelength coverage of the spectrographs dictate the parameter range here.

For bright and nearby sources, the photometric coverage is comprehensive and the data accurate, making the computation of reliable photo-z relatively easy. In contrast, with increasing faintness of the—possibly at high redshift—sources, the spectral energy distributions become less clearly defined (e.g., Hildebrandt et al. 2008). Fewer reliable source detections, larger statistical uncertainties associated with photometry, and an increasing number of upper limits, lead to poorly constrained SEDs (I09; S09). While this affects normal galaxies and AGNs in similar ways, the situation for the latter is complicated by the uncertainty in the relative contributions of the nuclear and host emission components.

These uncertainties were considered in Section 4.1, where we presented the application of our photo-z procedure to the *XMM*-COSMOS survey and the deeper C-COSMOS sample, and illustrated its limitations in correctly reproducing the properties of the faint end of the flux distribution.

For *XMM*-COSMOS, a large training spectroscopic sample allowed us to characterize the bright sources extremely well. Thus, when the same procedure was applied to the *Chandra* sources with similarly bright optical counterparts ($i^*_{\rm AB} < 22.5$), it provided a comparable accuracy and no further tuning of the library or the priors was required.

For the faint counterparts in *XMM*-COSMOS, no statistically meaningful spectroscopic sample was available; thus, no tuning for these sources was performed. The good agreement of the photo-z for the few *XMM* faint sources with spectroscopic redshifts suggested that the setup for the bright population could be extended to the entire X-ray sample. However, the significant increase in the spectroscopic sample with $i^*_{\rm AB} > 22.5$ for C-COSMOS indicated that the results for *XMM*-COSMOS in this range were likely the outcome of small number statistics and that a more careful study of the faint subsample was needed.

This demonstrated again the importance of the choice of the training sample for the quality of the photo-z. The accuracy and number of outliers calculated for a set of sources with spectroscopy can be used as a quality indicator for photo-z only if the sample without spectroscopy covers the same parameter space as the training sample. For a population dominated by sources fainter than the spectroscopic training sample, the quality of the photo-z is often overestimated.

6.2. Application to Other X-Ray Surveys

The strength of any photo-z estimation method is reflected mostly by how generally it can be applied. In Section 5, we illustrated how the procedure developed here for C-COSMOS led to an improvement in the photo-z for *XMM*-COSMOS (see Figure 9 and Table 3). For a similar test, we applied the method to the sources detected by *XMM* in another deep field, the Lockman Hole (Fotopoulou et al. 2011). The photometric coverage of the Lockman Hole has been extended to 22 broadbands from UV to mid-infrared (Rovilos et al. 2009, 2011), together with deep *HST*/ACS imaging. With these data, we have been able to reach an accuracy of $\sigma_{\rm NMAD} = 0.07$ and a fraction of outliers $\eta = 12.5\%$. The two values are comparable to the results of C-COSMOS, if the same photometric bands and depths as those used for the Lockman Hole are used and no variability correction is applied.

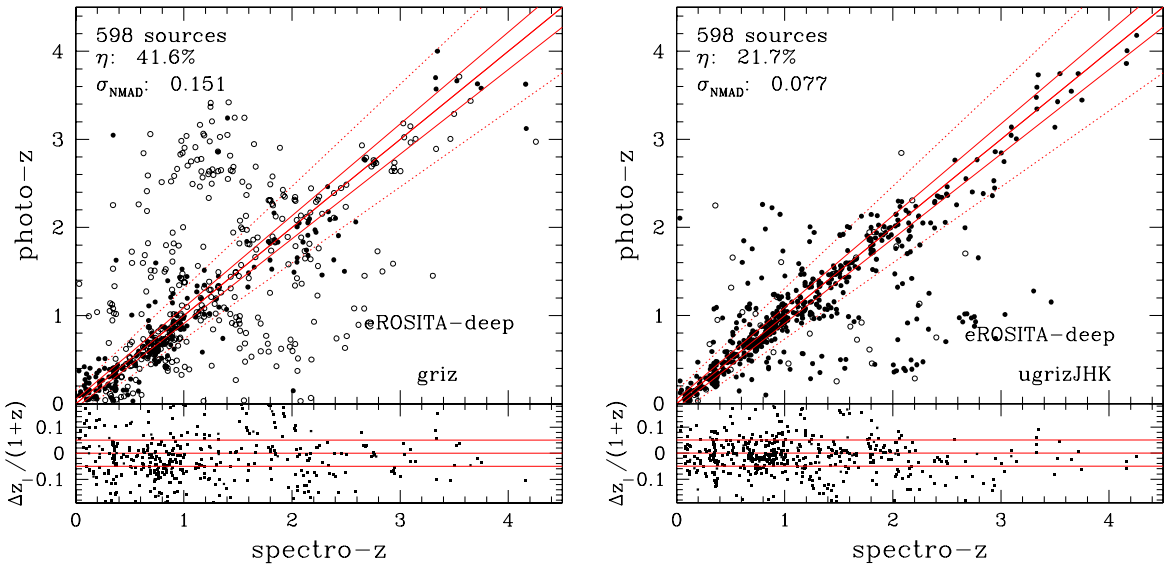

Figure 13. Photometric vs. spectroscopic redshifts for *XMM*-COSMOS sources at the X-ray depth of *eROSITA* Deep ($F_{0.5-2\,\mathrm{keV}} = 1 \times 10^{-15}$ erg cm^{-2} s^{-1}), using "*griz*" broadband photometry (left panel) and "*ugrizJHK*" (right panel). The high dispersion and fraction of outliers would render the photo-z computed with four bands, in the traditional way, unusable. Only the addition of "*u*" and "*JHK*" would allow reasonable results. This option should be considered at least for the deep part of the *eROSITA* survey.

This suggests that our procedure is robust and that its level of success is now dictated only by the available filters and depths. The procedure can be straightforwardly applied to the large number of deep multi-wavelength pencil-beam X-ray surveys such as *AEGIS-X* (Laird et al. 2009) and CDFS (Luo et al. 2010) or ECDFS (Cardamone et al. 2010). The study of the *AEGIS-X* field, which covers 0.67 deg^2, would benefit greatly from our procedure as the field is (1) wide enough to include some bright AGNs (needing AGN templates) and (2) deep enough ($F_{0.5-2\,\mathrm{keV}} = 5.3 \times 10^{-17}$ erg cm^{-2} s^{-1}) to include sources that are AGNs but for which the SED is more closely fit by normal galaxy templates. In addition, an accurate and merged photometric *AEGIS-X* catalog is now available (Barro et al. 2011).

ECDFS (0.25 deg^2) is probably the most deeply observed portion of the sky in terms of both imaging and spectroscopy. This has allowed a reconstruction of the SEDs of the sources and knowledge of the flux–redshift parameter space also at faint magnitudes. For the X-ray-detected sources, reliable photo-z has become available (Luo et al. 2010; Cardamone et al. 2010). By applying different methods and using partially different data sets (such as the additional photometry from 18 deep intermediate-band filters in Cardamone et al.), both groups obtain an accuracy of $\sigma < 0.01$. However, for 75 of the 169 sources without spectroscopy (i.e., 44%) that they have in common, the photo-z values differ by more than 0.2. Once again, it is clear that a good match between photometric and spectroscopic redshifts is not synonymous of univocal results.

Crucial information about the X-ray source population in the universe will also be provided by wide-field and all-sky missions, such as the *eROSITA* mission (Cappelluti et al. 2011), which is planned for launch in 2013 and is expected to detect several millions of AGNs brighter than $F_{0.5-2\,\mathrm{keV}} = 10^{-14}$ erg cm^{-2} s^{-1} in the all-sky. This flux limit is about a factor of 50 (10) brighter than the C-COSMOS (*XMM*-COSMOS) limit and the contamination by X-ray-emitting normal galaxies is likely negligible. Thus, the color–redshift degeneracy could in principle almost be eradicated by using the AGN-dominated S09 library for both the *QSOV* and the *EXTNV* samples.

However, the deep optical all-sky bands useful for the identification of the *eROSITA* sources will likely be limited to four to five broadbands from Pan-STARSS (Burgett & Kaiser 2009), LSST (Ivezic et al. 2006), Skymapper (Tisserand et al. 2008), and DES (DePoy et al. 2008; Mohr et al. 2008). While such an SDSS-like filter set can help to provide reliable photo-z for normal galaxies up to $z \sim 1$ (Oyaizu et al. 2008), it is insufficient for AGNs. In the left panel of Figure 13, we compare the photometric and spectroscopic redshifts of mock *eROSITA* sources. Here, we used the *XMM*-COSMOS sample cut at the X-ray flux above $F_{0.5-2\,\mathrm{keV}} = 10^{-15}$ erg cm^{-2} s^{-1} (*eROSITA* depth planned for the 2 × 100 deg^2 deep areas) and computed the photo-z using only *griz* photometry, as will be available from a very deep ($i = 26$ mag) Pan-STARRS filter set after a correction for variability. As expected, the fraction of outliers is large ($\eta = 41.5\%$) and the accuracy is well below what one would wish to achieve ($\sigma_{\mathrm{NAMD}} \sim 0.150$ for sources brighter than $F_{0.5-2\,\mathrm{keV}} = 10^{-15}$ erg cm^{-2} s^{-1}; $\sigma_{\mathrm{NAMD}} \sim 0.24$ for sources brighter than $F_{0.5-2\,\mathrm{keV}} = 10^{-14}$ erg cm^{-2} s^{-1}). Only with the addition of the "*u*" and "*JHK*" (the right panel of Figure 13) photometry will we be able to reach an accuracy that would allow us to use the measured photo-z for scientific studies. Without variability correction, the fraction of outliers would increase by additional 10%.

This clearly demonstrates the importance of multi-epoch observations and well-sampled SEDs (see also Benítez et al. 2009 for simulations). The availability of only broadband photometry will greatly limit the possibility of using SED fitting for computing photo-z for AGNs and new methods should be such as the inclusion of additional priors as the redshift or flux–redshift distributions (e.g., Benítez 2000 and Bovy et al. 2011, respectively). Only in this way will future X-ray surveys be able to maximize the insight they achieve in understanding AGN/galaxy (co)evolution.

7. CONCLUSIONS

It is generally believed that AGNs are playing a major role, although still to be fully understood, in galaxy formation and evolution. However, AGNs are rare compared to galaxies. Thus,

assembling large AGN redshift samples is a real challenge and requires much more telescope time than acquiring photometric data does. As a consequence, the main motivation for our work is the development of a better way to measure accurate photo-z for AGN-dominated galaxies using large photometric surveys.

In this paper, we have presented and thoroughly tested our methodology to derive photometric redshifts for X-ray sources. Our robust tuning of the photo-z technique for AGNs has been made possible thanks to (1) the sizable training spectroscopic sample spanning a large range in redshift, luminosity, and morphology of sources; (2) the multi-wavelength coverage; and (3) the correction for variability effects.

We presented the photo-z measurements of 1692 *Chandra*-detected sources and 1735 *XMM*-detected sources in the COSMOS field (869 sources are common to both surveys). While the former survey covers the central 0.9 deg^2 at a depth of $F_{(0.5-2\,\mathrm{keV})} = 1.9 \times 10^{-16}$ erg cm^{-2} s^{-1}, the latter is a factor of three to four shallower but covers the entire 2 deg^2 of the COSMOS field. For both samples, we have achieved an accuracy of $\sigma_{\mathrm{NMAD}} = 0.015$ and a fraction of outliers $\eta \sim 6\%$. In comparison with our previous analysis of the *XMM*-COSMOS sample (Salvato et al. 2009), we have shown that better results are obtained for faint, extended sources, which do not display optical variability, when a library of normal galaxies is used to fit their SEDs.

We have argued that the photo-z procedure adopted for X-ray sources in COSMOS can be applied to other X-ray surveys and will be a major asset for the scientific exploitation of any future large X-ray programs. The achievable accuracy is now limited only by both the depth of the photometric data and the number of the photometric bands available. For this reason, we propose that wide/all-sky X-ray surveys should invest substantially in multi-wavelength follow-up observations to enable researchers to fully exploit the potential of these surveys in studying AGN evolution.

We gratefully acknowledge the contributions of the entire COSMOS collaboration consisting of more than 100 scientists. More information about the COSMOS survey is available at http://www.astro.caltech.edu/~cosmos. We also acknowledge the use of STILTS and TOPCAT tools (Taylor 2005). We acknowledge the anonymous referee for helpful comments that improved the paper. M.S. and G.H. acknowledge support by the German Deutsche Forschungsgemeinschaft, DFG Leibniz Prize (FKZ HA 1850/28-1). F.C. was supported in part by NASA Chandra grant No. GO7-8136A, the Blancheflor Boncompagni Ludovisi foundation, and the Smithsonian Scholarly Studies. A.C., C.V., N.C., and F.F. acknowledge financial contribution from agreement ASI-INAF I/009/10/0.

Facilities: Keck:II, *HST*, VLT:Melipan, *CXO*, Sloan, *XMM*, Subaru

APPENDIX

DEFINITION OF ACRONYMS

HUDF:	HST Ultra Deep Field
AEGIS:	All-wavelength Extended Groth strip International Survey
COSMOS:	Cosmic Evolution Survey
GOODS:	Great Observatories Origins Deep Survey
ECDFS:	Extendend Chandra Deep Field South
CFHTLS:	Canadian-France-Hawaii Telescope Legacy Survey
LSST:	Large Synoptic Survey Telescope
WISE:	Wide-Field Infrared Survey Explorer (NOTE: all in italics)
FORS:	FOcal Reducer and low dispersion Spectrograph
VIMOS:	VIsible MultiObject Spectrograph
FLWO/FAST:	FAST spectrograph at the Fred Lawrence Whipple Observatory, Mount Hopkins, Arizona
SB templates:	Star-burst galaxy

REFERENCES

Aird, J., Nandra, K., Laird, E. S., et al. 2010, MNRAS, 401, 2531
Arnouts, S., Cristiani, S., Moscardini, L., et al. 1999, MNRAS, 310, 540
Barro, G., Pérez-González, P. G., Gallego, J., et al. 2011, ApJS, 193, 13
Becker, R. H., Fan, X., White, R. L., et al. 2001, AJ, 122, 2850
Bender, R., Appenzeller, I., Böhm, A., et al. 2001, in ESO Astrophysics Symposia, ed. S. Cristiani, A. Renzini, & R. E. Williams (Berlin: Springer-Verlag), 96
Benítez, N. 2000, ApJ, 536, 571
Benítez, N., Moles, M., Aguerri, J. A. L., et al. 2009, ApJ, 692, L5
Bertin, E., & Arnouts, S. 1996, A&AS, 117, 393
Bovy, J., Myers, A. D., Hennawi, J. F., et al. 2011, arXiv:1105.3975
Brusa, M., Civano, F., Comastri, A., et al. 2010, ApJ, 716, 348
Bruzual, G., & Charlot, S. 2003, MNRAS, 344, 1000
Burgett, W., & Kaiser, N. 2009, in Proc. Advanced Maui Optical and Space Surveillance Technologies Conference, ed. S. Ryan (Kihei, HI: Maui Economic Development Board), E39
Calzetti, D., Armus, L., & Bohlin, R. C. 2000, ApJ, 533, 682
Capak, P., Aussel, H., Ajiki, M., et al. 2007, ApJS, 172, 99
Cappelluti, N., Brusa, M., Hasinger, G., et al. 2009, A&A, 497, 63
Cappelluti, N., Predehl, P., Böhringer, H., et al. 2011, Mem. Soc. Astron. Ital. Suppl., 17, 159
Cardamone, C. N., van Dokkum, P. G., Urry, C. M., et al. 2010, ApJS, 189, 270
Civano, F., Brusa, M., Comastri, A., et al. 2011, arXiv:1103.2570
Cuillandre, J.-C., & Bertin, E. 2006, in Proc. Annual Meeting of the French Society of Astronomy and Astrophysics, ed. D. Barret et al. (Paris: SF2A), 265
Davis, M., Guhathakurta, P., Konidaris, N. P., et al. 2007, ApJ, 660, L1
DePoy, D. L., Abbott, T., Annis, J., et al. 2008, Proc. SPIE, 7014, 13
Duval, V. G., Irace, W. R., Mainzer, A. K., & Wright, E. L. 2004, Proc. SPIE, 5487, 101
Elvis, M., Civano, F., Vignali, C., et al. 2009, ApJS, 184, 158
Fan, X., Narayanan, V. K., Lupton, R. H., et al. 2001, AJ, 122, 2833
Fan, X., Strauss, M. A., Becker, R. H., et al. 2006, AJ, 132, 117
Fontanot, F., Cristiani, S., Monaco, P., et al. 2007, A&A, 461, 39
Fotopoulou, S., Salvato, M., Hasinger, G., et al. 2011, ApJS, in press (arXiv:1110.0960)
Giavalisco, M., Ferguson, H. C., Koekemoer, A. M., et al. 2004, ApJ, 600, L93
Grogin, N. A., Kocevski, D. D., Faber, S. M., et al. 2011, arXiv:1105.3753
Hasinger, G., Cappelluti, N., Brunner, H., et al. 2007, ApJS, 172, 29
Hildebrandt, H., Wolf, C., & Benítez, N. 2008, A&A, 480, 703
Hoaglin, D. C., Mosteller, F., & Tukey, J. W. (ed.) 1983, Understanding Robust and Exploratory Data Analysis (Wiley Series in Probability and Mathematical Statistics; New York: Wiley)
Hopkins, P. F., Hernquist, L., Cox, T. J., & Kereš, D. 2008, ApJS, 175, 356
Ilbert, O., Arnouts, S., McCracken, H. J., et al. 2006, A&A, 457, 841
Ilbert, O., Capak, P., Salvato, M., et al. 2009, ApJ, 690, 1236
Ilbert, O., Salvato, M., Le Floc'h, E., et al. 2010, ApJ, 709, 644
Ivezic, Z., Tyson, A. J., Strauss, M. A., et al. 2006, BAAS, 38, 1017
Koekemoer, A. M., Alexander, D. M., Bauer, F. E., et al. 2004, ApJ, 600, L123
Koekemoer, A. M., Aussel, H., Calzetti, D., et al. 2007, ApJS, 172, 196
Koekemoer, A. M., Faber, S. M., Ferguson, H. C., et al. 2011, arXiv:1105.3754
Laird, E. S., Nandra, K., Georgakakis, A., et al. 2009, ApJS, 180, 102
Leauthaud, A., Massey, R., Kneib, J.-P., et al. 2007, ApJS, 172, 219
Lehmer, B. D., Brandt, W. N., Alexander, D. M., et al. 2005, ApJS, 161, 2
Lilly, S. J., Le Brun, V., Maier, C., et al. 2009, ApJS, 184, 218
Lilly, S. J., Le Fèvre, O., Renzini, A., et al. 2007, ApJS, 172, 70
Luo, B., Brandt, W. N., Xue, et al. 2010, ApJS, 187, 560
Maccacaro, T., Gioia, I. M., Wolter, A., Zamorani, G., & Stocke, J. T. 1988, ApJ, 326, 680
McCracken, H. J., Capak, P., Salvato, M., et al. 2010, ApJ, 708, 202

Menci, N., Fiore, F., Puccetti, S., & Cavaliere, A. 2008, ApJ, 686, 219
Mohr, J. J., Adams, D., Barkhouse, W., et al. 2008, Proc. SPIE, 7016, 17
Norris, R. 2010, BAAS, 36, 1127
Oyaizu, H., Lima, M., Cunha, C. E., et al. 2008, ApJ, 674, 768
Polletta, M., Tajer, M., Maraschi, L., et al. 2007, ApJ, 663, 81
Predehl, P., Andritschke, R., Bornemann, W., et al. 2007, Proc. SPIE, 6686, 36
Prescott, M. K. M., Impey, C. D., Cool, R. J., & Scoville, N. Z. 2006, ApJ, 644, 100
Prevot, M. L., Lequeux, J., Prevot, L., Maurice, E., & Rocca-Volmerange, B. 1984, A&A, 132, 389
Puccetti, S., Vignali, C., Cappelluti, N., et al. 2009, ApJS, 185, 586
Rovilos, E., Burwitz, V., Szokoly, G., et al. 2009, A&A, 507, 195
Rovilos, E., Fotopoulou, S., Salvato, M., et al. 2011, A&A, 529, 135
Salvato, M., Hasinger, G., Ilbert, O., et al. 2009, ApJ, 690, 1250
Sanders, D. B., Salvato, M., Aussel, H., et al. 2007, ApJS, 172, 86
Scoville, N., Abraham, R. G., Aussel, H., et al. 2007, ApJS, 172, 38
Taylor, M. B. 2005, in ASP Conf. Ser. 347, Astronomical Data Analysis Software and Systems XIV, ed. P. Shopbell, M. Britton, & R. Ebert (San Francisco, CA: ASP), 29
Tisserand, P., Keller, S., Schmidt, B., & Bessell, M. 2008, in Galaxies in the Local Volume, ed. B. S. Koribalski & H. Jerjen (Dordrecht: Springer), 337
Trump, J. R., Impey, C. D., McCarthy, P. J., et al. 2007, ApJS, 172, 383
Veron-Cetty, M.-P., & Veron, P. 2001, A&A, 374, 92
Williams, R. E., Blacker, B., Dickinson, M., et al. 1996, AJ, 112, 1335
Willott, C. J., McLure, R. J., & Jarvis, M. J. 2003, ApJ, 587, L15
Wolf, C., Meisenheimer, K., Kleinheinrich, M., et al. 2004, A&A, 421, 913
Wolf, C., Meisenheimer, K., Rix, H., et al. 2003, A&A, 401, 73
Wolf, C., Meisenheimer, K., Röser, H.-J., et al. 2001, A&A, 365, 681
Wright, N. J., Drake, J. J., & Civano, F. 2010, ApJ, 725, 480
Zamojski, M. A., Schiminovich, D., Rich, R. M., et al. 2007, ApJS, 172, 468